Role of Extracellular Glutamic Acids in the Stability and Energy Landscape of Bacteriorhodopsin

K. Tanuj Sapra,* Jana Doehner,* V. Renugopalakrishnan,† Esteve Padrós,‡ and Daniel J. Muller*
*Biotechnology Center, University of Technology, Dresden, Germany; †Children's Hospital, Harvard Medical School, Boston, Massachusetts; and ‡Unitat de Biofísica, Departament de Bioquímica i de Biologia Molecular, Facultat de Medicina, and Centre d'Estudis en Biofísica, Universitat Autonoma de Barcelona, Barcelona, Spain

ABSTRACT Bacteriorhodopsin (BR), a specialized nanomachine, converts light energy into a proton gradient to power *Halobacterium salinarum*. In this work, we analyze the mechanical stability of a BR triple mutant in which three key extracellular residues, Glu^{9}, Glu^{194}, and Glu^{204}, were mutated simultaneously to Gln. These three Glu residues are involved in a network of hydrogen bonds, in cation binding, and form part of the proton release pathway of BR. Changes in these features and the robust photocycle dynamics of wild-type (WT) BR are apparent when the three extracellular Glu residues are mutated to Gln. It is speculated that such functional changes of proteins go hand in hand with changes in their mechanical properties. Here, we apply single-molecule dynamic force spectroscopy to investigate how the Glu to Gln mutations change interactions, reaction pathways, and the energy barriers of the structural regions of WT BR. The altered heights and positions of individual energy barriers unravel the changes in the mechanical and the unfolding kinetic properties of the secondary structures of WT BR. These changes in the mechanical unfolding energy landscape cause the proton pump to choose unfolding pathways differently. We suggest that, in a similar manner, the changed mechanical properties of mutated BR alter the functional energy landscape favoring different reaction pathways in the light-induced proton pumping mechanism.

INTRODUCTION

Bacteriorhodopsin (BR) functions as a light-driven proton pump in the outer membrane of the archaebacterium *Halobacterium salinarum*, and provides a photosynthetic source of energy when the oxygen concentration drops below the threshold level capable of sustaining respiration (1). BR, the main constituent of purple membrane in the outer membrane, assembles into trimers within a hexagonal lattice of 6.2 nm. BR consists of seven transmembrane (TM) α-helices (2) surrounding the photoactive retinal covalently linked to Lys^{216} by a Schiff base (3,4). Upon absorption of light, the retinal isomerizes from the all-*trans* to the 13-*cis* (5) conformation accompanied by a series of structural changes that are characterized by an alteration in the absorption spectrum and the refractive index of the protein (6). During this process, a proton is transferred across the purple membrane, thereby providing energy to power the bacterium.

Single-molecule force spectroscopy (SMFS) has been established as a tool to mechanically unfold membrane proteins (7). The resulting force-distance (F-D) spectrum detects and locates the strength of molecular interactions that stabilize certain structural regions of the membrane protein. Dynamic SMFS (DFS) probes these interactions at different timescales to extract the defining parameters of prominent energy barriers. These energy barriers define the kinetic stability of the structural segments in the membrane protein, and build part of the energy landscape along the force-driven unfolding pathway chosen by the protein (8,9). Recently, we and others have shown that the energy landscape of a protein is sculpted by the mechanical properties of its structural segments (10,11). The rigidity of structural segments may be crucial in guiding the conformational changes required for the protein's function. Determination of the energy landscape thus becomes important in understanding the structural stability and functional dynamics of a protein.

Here, we put forth a hypothesis that a protein showing altered functionality would also show altered mechanical characteristics. To test this hypothesis we performed single-molecule DFS measurements on a BR triple mutant E9Q/E194Q/E204Q (3Glu BR; see Fig. 1). Glu residues located in the extracellular region of BR, Glu^{9}, Glu^{194}, and Glu^{204} are involved in a network of hydrogen bonds, and are suggested to have a role in cation binding (12). More importantly these residues form part of the proton release pathway (13–15) and hence are important for BR functioning. The importance of the extracellular Glu residues and their photoelectrochemical role in BR (16–20) provides the rationale for mutating Glu to Gln. In this work, we characterize the structural properties of the 3Glu mutant, which has been assayed as a light harvester for solar cell applications. Preliminary results show better photoelectric performance of 3Glu BR as compared to wild-type (WT) BR (67). This advantage may result from a less charged extracellular surface due to the presence of Gln side chains instead of Glu, and thus an easy interaction with the TiO_2 surface. However, these mutations could also lead to changes in the molecular interactions responsible for the

Submitted February 20, 2008, and accepted for publication June 11, 2008.

Address reprint requests to Daniel J. Muller, E-mail: mueller@biotec.tu-dresden.de; or to K. Tanuj Sapra, E-mail: sapra@biotec.tu-dresden.de.

Jana Doehner's present address is Institute of Pharmacology and Toxicology, Winterthurerstr. 190, University of Zurich, Zurich, Switzerland.

Editor: Anthony Watts.

0006-3495/08/10/3407/12 $2.00

doi: 10.1529/biophysj.108.131904

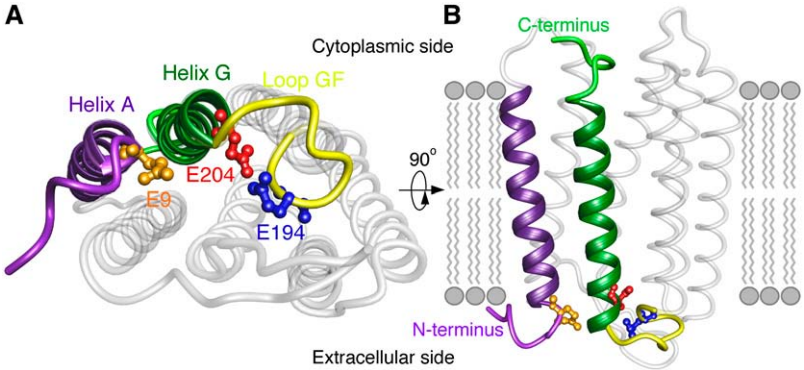

FIGURE 1 Mapping Gln mutations E9Q/E194Q/E204Q (3Glu BR) in BR. WT BR (PDB ID: 1AT9) as viewed from the extracellular surface (*A*) and side view from the membrane (*B*). Mutated residues, E9 (*orange*), E194 (*blue*), and E204 (*red*) are shown in ball-and-stick representation. E9 is located at the extracellular end of α-helix A (*purple*), E194 in extracellular loop GF (*yellow*), and E204 at the extracellular side of α-helix G (*dark green*).

formation of structural units. Therefore, it was of interest to evaluate the effect of these mutations on the mechanical stability related to the proton transport function.

DFS could detect changes in the molecular interactions, energy landscape, and mechanical properties of BR upon substitution of extracellular Glu residues. Consequently, the unfolding pathways of 3Glu BR were different from those preferred by WT BR. Protein unfolding can be described by reaction pathways chosen along energy landscapes. Here, we suggest that the changes detected in the energy landscape may also funnel the protein function differently.

MATERIALS AND METHODS

Preparation of 3Glu BR

Purple membranes containing WT BR were isolated from *H. salinarum* strain S9 as described (21). The triple mutant E9Q/E194Q/E204Q, 3Glu BR, was obtained as follows: the gene encoding BR, bop gene, subcloned in pUC119 as a 1.2 kb *Bam*HI/*Hin*dIII fragment (a gift from Dr. R. Needlemann), was used as a template for mutagenesis. Single mutants were obtained by PCR site-directed mutagenesis and amplified in the *Escherichia coli* TG1 strain. Screening of the mutants was performed by DNA sequencing. 3Glu BR was constructed by cloning single Gln mutants together taking advantage of unique restriction sites. It was transformed and expressed in the *H. salinarum* L33 strain with help of the shuttle plasmid pXLNovR. Mutations were confirmed from *H. salinarum* transformants by sequencing the bop gene from isolated DNA.

SMFS and DFS of 3Glu BR

SMFS was used to unfold individual BR molecules as described (22,23). As a first step, ~2 μL of BR containing membrane patches, diluted to a concentration of ~0.4 mg/mL, were adsorbed in 300 mM KCl, 20 mM Tris (pH 7.8) onto a freshly cleaved mica surface. After locating the protein membrane patches the atomic force microscope (AFM) stylus was pushed onto the membrane surface at a constant force of ~1 nN for ~0.5^{-1} s. This forced the terminal end of BR to attach to the stylus via nonspecific interactions forming a molecular bridge (22). Withdrawal of the AFM stylus stretched this molecular bridge, exerting a force at the membrane protein. At sufficiently high forces, the sequential unfolding of structural segments of the protein was induced. Differences in unfolding BR from the N- and C-terminal ends have been characterized previously (24). In this study, BR was unfolded by pulling from the C-terminal region as determined by fitting force peaks of F-D curves to the wormlike chain (WLC) model.

DFS on 3Glu BR was performed at six different pulling speeds of 100, 350, 700, 1310, 2320, and 5230 nm/s. All DFS experiments were conducted under identical physiological conditions, BR was embedded into the native purple membrane, and pH, electrolyte concentration, and temperature of the buffer solution were kept constant. Spring constants of the 200-μm-long AFM cantilevers (NPS, Veeco Metrology, Santa Barbara, CA; nominal spring constant ~0.08 N/m) were calibrated in buffer solution using the equipartition theorem (25,26). All experiments on 3Glu BR were performed using cantilevers from the same wafer, and the measured spring constants were within ~10% of each other. To minimize errors due to cantilever spring constant deviations in DFS measurements, 3Glu BR was unfolded at a specific speed using at least three different cantilevers. The number of F-D curves collected for 3Glu BR was 127 (100 nm/s), 105 (350 nm/s), 130 (700 nm/s), 125 (1310 nm/s), 130 (2620 nm/s), and 100 (5230 nm/s). WT BR data were taken from a recent study (27), and the number of curves was 10 (10 nm/s), 84 (50 nm/s), 79 (87.2 nm/s), 165 (654 nm/s), 121 (1310 nm/s), 23 (2620 nm/s), and 51 (5230 nm/s). All experiments were performed at room temperature using a Picoforce (dI-Veeco) AFM equipped with the PF scanner.

DATA ANALYSIS

Selection of force-distance curves

We have previously established a robust method to identify F-D curves resulting from the mechanical unfolding of single BR molecules from their C-terminal end (22,23). In short, this method relies on the fact that F-D curves exhibiting an overall length between 60 and 70 nm reflect complete unfolding and extension of BR molecules attached by their C-terminal end to the AFM stylus. All curves exhibiting this length were selected and aligned manually. Every peak of a single F-D curve was fitted using the WLC model with a persistence length of 0.4 nm and a monomer length of 0.36 nm (28). The contour lengths obtained from the WLC fits give the number of extended amino acids at each peak and allow us to assign unfolding events to structural segments of BR, as described before (23). To measure the unfolding force of each structural segment, every event of each curve was analyzed.

Phenomenological model versus microscopic models

Recently, Dudko et al. (29) proposed a unified microscopic model for optimum fitting to the data obtained at increasing loading rates. This model accounts for the discrepancy between the two microscopic models proposed previously

(30,31), and also between the microscopic models and the phenomenological model of Evans (9). For the model systems titin and RNA, this unified framework predicts consistent values of the distance of the transition state from the folded state (x_u) and the unfolding rate (k_u) when using the microscopic theories. Although the value of x_u obtained from the phenomenological method is quite close to that derived from the microscopic models, the value of k_u is off by approximately an order of magnitude when compared to the microscopic models. However, to our knowledge, the validity of the microscopic model lacks a firm confirmation by independent experimental verification. In the light of the fact that small changes in x_u are sensitively linked to k_u (32), it is not surprising that the values of k_u change by an order of magnitude. An order-of-magnitude difference is, therefore, not a considerable one, given the fact that Dudko et al. do not give errors on the reported values. Importantly, in this study we considered two values of k_u different only when the difference is two orders-of-magnitude or more. Moreover, the loading rates in our experiments were in the intermediate range so as not to introduce any curvature in the mean rupture force, $\langle F \rangle$, versus $\log_e$(loading rate) plot for which the microscopic models seem to work better. Thus, here we chose to use Evans' phenomenological theory based on Bell's seminal work (33).

Calculating x_u and k_u from DFS

DFS with AFM involves unfolding a protein at increasing pulling speeds (34). Plotted as the most probable unfolding force versus $\log_e$(loading rate), the force spectrum maps the most prominent energy barriers in the energy landscape along the force-driven pathway (8,35). The most probable unfolding force, F_p, can be described as

$$F_p = \frac{k_B T}{x_u} \ln\left(\frac{x_u r_f}{k_B T k_u}\right), \quad (1)$$

where k_B is the Boltzmann constant, T is the temperature, x_u denotes the distance from the free energy minimum to the transition barrier, k_u is the unfolding rate under no applied force, and r_f is the loading rate. Instead of the most probable force we plotted the mean force, $\langle F \rangle$, versus $\log_e$(loading rate). A least-squares fit of the data using Eq. 1 provides x_u and k_u.

Estimation of transition barrier heights and rigidity of structural segments

The barrier height, ΔG_u^*, between a transition state and a folded state was estimated using the Arrhenius equation $\Delta G_u^* = -k_B T \times \ln(\tau_A/\tau_0)$, where τ_0 denotes the lifetime of the intermediate state under zero loading ($\tau_0 = 1/k_u$), and $1/\tau_A$ the Arrhenius frequency factor (9,36). A typical value of τ_A in protein dynamics is 10^{-9} s (37). The errors of k_u were propagated to estimate the errors in ΔG_u^* calculation. The spring constant, κ, was determined using the formula $\kappa = 2 \times \Delta G_u^*/x_u^2$ (11,38,39). This value was taken as an estimate of protein rigidity in the direction of pulling. The errors of ΔG_u^* and x_u were propagated in the estimation of errors of κ.

Probability calculation of unfolding pathways

To determine the effect of mutations on the unfolding pathways we calculated the probability of all the unfolding pathways of each structural segment of 3Glu BR at every unfolding speed. Table 1 compares the probabilities of unfolding pathways of 3Glu BR (700 nm/s) with WT BR (654 nm/s). Each pathway was codified as a string of 0 and 1, where 1 corresponds to the sequence position denoting the presence of a peak and 0 corresponds to the sequence position where the given peak was missing. The standard errors in the probability of the unfolding pathways were calculated using the equation $\sqrt{(p(1-p)/n)}$, where p is the probability, and n the total number of F-D curves.

It is well known that the probability of unfolding pathways of a protein changes with loading rates (27,40). However, the difference in loading rates at a specific speed owing to a calibration error of 10–20% in the spring constants of different cantilevers is less than the difference in the loading rates at different speeds observed in previous studies (27,40). Therefore, we believe that the observed changes in the probability of the unfolding pathways in our experiments are not due to the differences in loading rates arising from the calibration error in the spring constants. Recently it was shown that different spring constants (loading rates) could force a polypeptide to unfold via different pathways (41). However, the spring constants of the cantilevers used for those measurements were an order-of-magnitude different. The authors did not observe different unfolding pathways while using one type of cantilever, which had a calibration error of 20%. In addition, previous DFS experiments on WT BR and five different BR mutants using similar cantilevers all showed the same unfolding pathways and no new ones (27,40). We, therefore, firmly believe that the detection of a new unfolding intermediate in this study is not owing to errors in spring constant calibration.

RESULTS

Gln mutations guide BR to unfold via a new intermediate

Mechanical unfolding of membrane proteins by SMFS gives rise to F-D curves (7,42). Each force peak in the F-D curve represents the unfolding of a certain structural segment constituted by complete or partial TM α-helices, polypeptide loops, a single TM α-helix and loops, or two TM α-helices and a connecting loop. The sequence of force peaks in a single F-D curve denotes which structural segments establish the intermediate states in the unfolding pathway of the membrane protein (23,27). We replaced three Glu residues of BR at

TABLE 1 Probability of unfolding pathways of 3Glu and WT BR

	Peak position from C-terminus (amino acids, aa) Position from N-terminus (aa)											Probability (%)	
Structural segments	26 222	36 200	51 194	88 159	94 144	105 129	148 101	158 79	175 63	219 30	232 17	WT BR	3Glu BR
Helix G-1, loop GF-2, helix F-2	1	1	1									10 ± 2	31 ± 4
Helix G-2, loop GF and helix F-2	1	1	0									5 ± 2	4 ± 2
Helix G and loop GF, helix F-4*	1	0	1									3 ± 1	4 ± 2
Loop GF-1, helix F-1	0	1	1									29 ± 4	15 ± 3
Loop GF and helix F-1	0	1	0									13 ± 3	10 ± 3
Helix F-3†	0	0	1									0	15 ± 3
Helices E and D				1	0	0						25 ± 3	30 ± 4
Helix E, helix D-1				1	0	1						39 ± 4	32 ± 4
Part helix E, part helix E, helix D-2				1	1	1						22 ± 3	20 ± 4
Part helix E, part helix E and helix D				1	1	0						15 ± 3	18 ± 3
Helices B and C							1	0	0			33 ± 4	17 ± 3
Helix C and loop BC, helix B-1							1	0	1			39 ± 4	34 ± 4
Helix C-2, loop BC, helix B-2							1	1	1			10 ± 2	17 ± 3
Helix C-1, loop BC and helix B							1	1	0			18 ± 3	32 ± 4
Helix A and N-terminus										1	0	97 ± 1	59 ± 4
Helix A, N-terminus										1	1	3 ± 1	41 ± 4

Unfolding pathways of 3Glu and WT BR were constructed from the unfolding intermediates. The probability occurrence of the unfolding pathways changed for 3Glu BR as compared to WT BR. A comparison of the occurrence probabilities (mean ± SE) between the 3Glu and WT BR is shown for pulling speed 700 nm/s. Due to changes in intramolecular interactions these probabilities could vary considerably for certain unfolding pathways. Note that ''1'' denotes the presence of a peak in the F-D curve and hence the unfolding of the structural segment corresponding to the peak in the unfolding pathway, and ''0'' denotes a missing peak and the absence of the corresponding structural segment in the unfolding pathway. It is important to mention that the presence of a force peak at the same position does not necessarily denote identical unfolding events. For example, the appearance of a force peak at amino-acid position 88 followed by a force-peak at position 148 denotes the unfolding of TM helices E and D together constituting one pathway, whereas a peak at position 88 followed by a peak at position 105 denotes the unfolding of TM helix E alone, thus constituting a different pathway (see Fig. 3). This combination of stochastic unfolding events gives rise to different unfolding pathways.

*Due to the very low frequency of occurrence of these pathways, we do not report the unfolding forces.

†New pathway detected in 3Glu BR (Fig. 3).

positions 9, 194, and 204 with Gln (Fig. 1) to explore their role in the BR structure. A change in interactions due to mutations can be detected by the introduction of a new or deletion of an existing structural segment. F-D curves resulting from the mechanical unfolding of 3Glu BR showed the presence of well-defined force peaks at amino acid positions previously detected for WT BR (Fig. 2, Supplementary Material Fig. S2 *A* in Data S1) (23). All positions of individual peaks remained the same independent of the pulling speed (Fig. S2, *B–F* in Data S1). This suggested that the substitution of Glu by Gln did not change the positions of the structural segments stabilized in BR.

Focusing on TM helices G and F, which host the mutations E194Q and E204Q, several unfolding pathways were observed (Fig. 3, Table 1). The structural segments constituted by helices G and F in 3Glu BR unfolded via all the five pathways observed before for WT BR (23). Interestingly, we observed the presence of an additional combination of force-peaks denoting a new unfolding pathway of helices G and F. In the new pathway, the C-terminal was stretched triggering

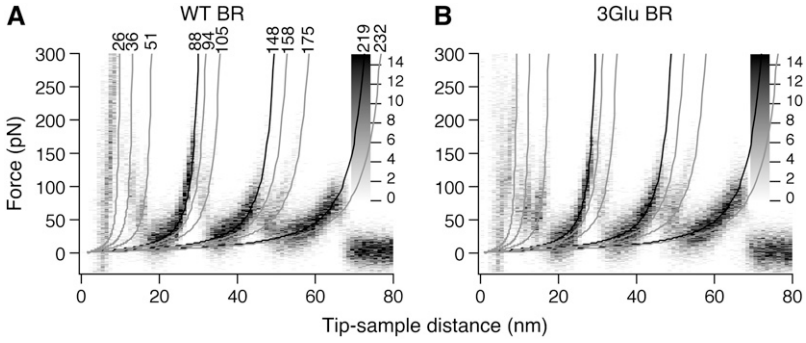

FIGURE 2 Superimpositions of F-D traces of 3Glu and WT BR. The superimpositions of F-D traces recorded by SMFS enhance common unfolding patterns of single BRs and demonstrate the reproducibility of the unfolding pathways. Superimpositions are fitted with the WLC model (*black lines*) to show the occurrence of main peaks (occurrence ~100%) indicating stretched polypeptides corresponding to lengths of 88, 148, and 219 amino acids. Gray lines denote WLC fits of side peaks (occurrence ≪100%) corresponding to stretched polypeptide lengths of 26, 36, 51, 94, 105, 158, 175, and 232 amino acids. Many of these side peaks are masked in the noise of the superimposition. Major and minor force peaks of 3Glu and WT BR occurred at the same positions (Fig. S2 in Data S1). The grayscales allow us to statistically interpret the superimpositions. F-D traces superimposed were collected at a pulling speed of 600 nm/s for WT BR (*A*) and 700 nm/s for 3Glu BR (*B*). To show the peaks clearly in each case only 43 curves are superimposed.

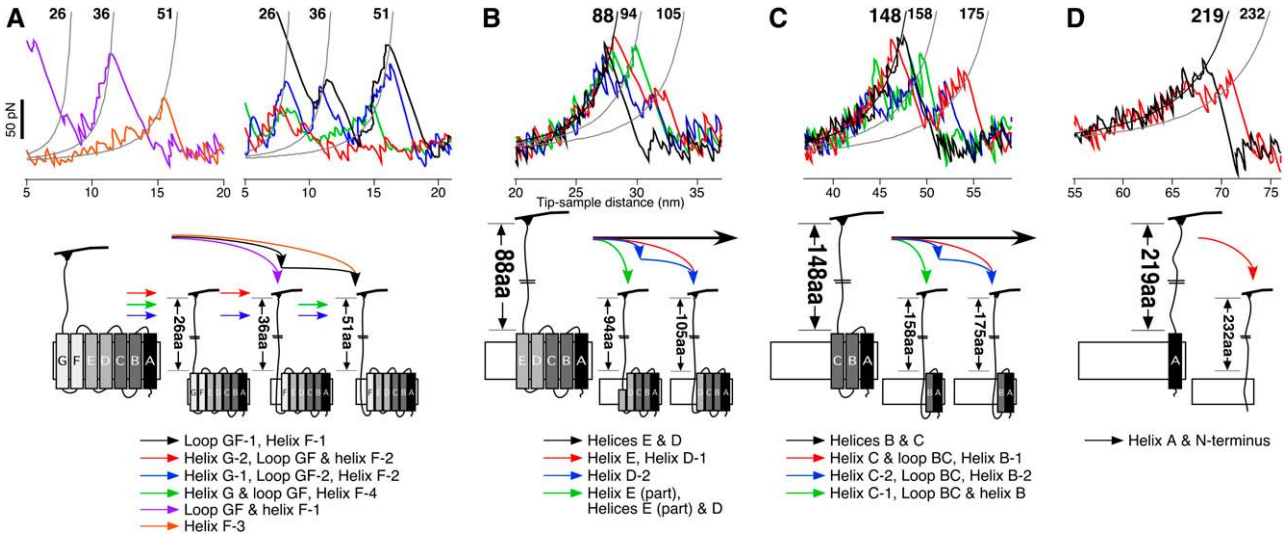

FIGURE 3 Unfolding pathways of 3Glu BR. Superimposition of F-D curves of 3Glu and WT BR (Fig. 2) can mask the side peaks occurring at a much lower probability (<50%) due to the noise in the superimposition. A closer look at individual F-D curves reveals these side peaks. (*A–D*) Individual peaks in F-D curves fitted by the WLC model denote different structural intermediates of the unfolding pathways via which 3Glu BR could unfold (23). Each WLC fit reveals the length of the stretched polypeptide (given in amino acids), which is used to locate the interaction in BR. The distance between two subsequent force peaks denotes the length of the structural segment constituting the unfolding barrier. The lower panels in *A–D* denote the structural segments stabilized by the molecular interactions detected by the force peaks. The combination of different force peaks detected in a F-D curve constitutes the unfolding pathway of the protein. All possible pathways observed in WT BR were also detected for 3Glu BR. Besides these, one new pathway was detected for unfolding of TM helices G and F in 3Glu BR (*orange trace* in *A*). (*A*) The arrows denote the sequence of unfolding events of different structural segments. For clarity not all force peaks are shown together and some of the arrows denoting the unfolding sequence of structural segments are shown separately. (*B–D*) Black arrows denote secondary structure elements that unfolded together. These structures could also unfold via alternative pathways as shown by differently colored arrows. Unfolding intermediates for 3Glu and WT BR remained the same, although the occurrence probabilities showed a dramatic change in certain cases (Table 1). Colors of the force peaks (*upper panel*) correspond to that of the arrows (*lower panel*) denoting the unfolding of different structural segments. The number after a structural segment, e.g., loop GF-1, helix F-1, in the lower panel denotes the pathway number of the structural segment. Black WLC fits are to the main peaks, and gray WLC fits to the side peaks.

the unfolding of helix G with loop GF, followed by the unfolding of helix F with loop FE (peak at amino acid 51). This pathway, characterized by the presence of only one force-peak at amino acid 51, occurred with a probability of 15% (Table 1). In addition, several other unfolding pathways, common to both 3Glu and WT BR, showed noticeable changes in their occurrence probabilities. Overall, these results suggest that Gln substitutions at positions 9, 194, and 204 forced BR to populate different unfolding pathways.

In a recent study we have reported the effect of oligomeric assemblies on the mechanical stability and unfolding pathways of BR (43). In that study we did not detect new unfolding intermediates in dimeric or monomeric assemblies, although the population distribution of the unfolding intermediates did change when compared to trimeric WT BR. This suggests that a change in the oligomeric assembly, although influences the population distribution of the unfolding intermediates, need not necessarily introduce a new unfolding intermediate. Also, the frequency of successful events (defined by the picking of a BR molecule), in the case of BR monomers, was much lower as compared to WT BR—a good indication of the low packing density of BR molecules in the former sample (43). In this study we detected a new unfolding intermediate with a high occurrence (15%). This unfolding intermediate could be localized to the structural segments hosting the mutations. None of the mutations was located at the protein-protein interface so as to have a detrimental effect on the lattice assembly. Moreover, the frequency of successful picking events of 3Glu BR was similar to that of WT BR (~10%). It is also imperative to mention that a recent NMR study speculated that mutating the extracellular Glu residues of BR led to the disappearance of some interhelical interactions and the creation of extra space either by the disrupted or the disorganized hexagonally packed lattice structure (44). However, a major stress of the NMR study was the disorganized extracellular region due to the extracellular Glu mutations. During the AFM experiments we did not image any unusual pattern in the BR patches (data not shown). Thus, we reckon that the extracellular 3Glu mutations in this study did not significantly alter the lattice assembly of BR, and that the observed changes in the unfolding pathways are not due to destruction of the WT BR assembly as observed in our previous study (43).

Mechanical, kinetic, and energetic properties of 3Glu BR

Mechanical stability of 3Glu BR is different from WT BR

The force required to unfold an individual structural segment reflects the strength of inter- and intramolecular interactions.

It has been shown that these interactions depend sensitively on the pH and electrolyte of the buffer solution (23), temperature (45), ligand binding (46), oligomeric assembly of the membrane protein (43,47), as well as on single point mutations in the structural segments (40). Moreover, changes in interactions have been shown to reshape the energy landscape of membrane proteins (40,48). The influence of the three mutations, E9Q/E194Q/E204Q, on the interactions established in BR was determined by comparing the unfolding forces of 3Glu BR with those of WT BR. DFS was employed to unfold 3Glu BR at pulling speeds of 100, 350, 700, 1310, 2320, and 5320 nm/s. A semilogarithmic plot of $\langle F \rangle$ versus $\log_e$(loading rate) gives an estimate of the distance between the energy minimum of the intermediate state and its transition state barrier, x_u, and the unfolding rate, k_u (Fig. 4, Fig. S1 in Data S1).

The forces required to individually unfold TM helix G (Fig. 4 *A*) and loop GF via two pathways (Fig. 4, *B* and *C*, respectively) were considerably lower for 3Glu BR as compared to WT BR. The structural segment loop GF together with TM helix F, which hosted mutations E194Q and E204Q, unfolded cooperatively via two pathways (Fig. 3). In both pathways unfolding occurred at slightly higher forces in 3Glu BR (Fig. 4 *D*, Fig. S1 *C* in Data S1), as compared to WT BR.

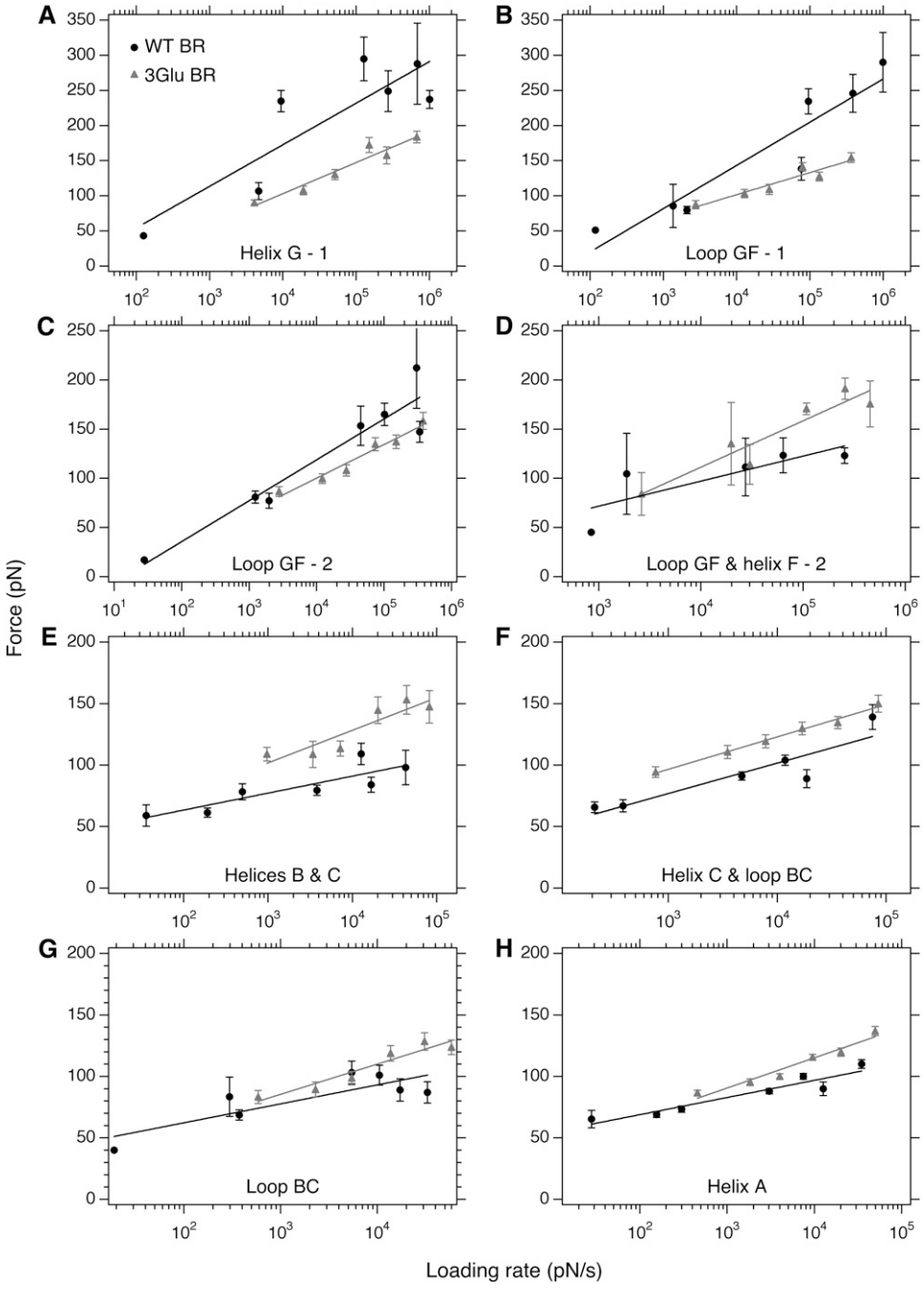

FIGURE 4 Dynamic force spectroscopy of 3Glu and WT BR. Unfolding a membrane protein at different speeds helps to determine details of its underlying energy landscape. 3Glu BR was unfolded using SMFS at pulling speeds of 100, 350, 700, 1310, 2620, and 5230 nm/s. (*A–H*) All structural segments of 3Glu BR (*gray triangles*) showed a change in unfolding forces as compared to WT BR (*solid circles*). The slope of the semilogarithmic plot of the unfolding forces versus loading rates gave the values of x_u and k_u of each structural segment in the unfolding pathway. As shown, the slopes of most stable structural segments, helix G-1 (*A*), loop GF-1 (*B*), loop GF and helix F-2 (*D*), helices B and C (*E*), loop BC (*G*), and helix A (*H*) in the 3Glu BR (*gray*) showed a change when compared to WT BR (*solid*). These structural segments showed an intersection in the slopes denoting a crossover in their stabilities at a specific loading rate. Values of x_u and k_u for both, 3Glu and WT BR, are given in Table 2. Data points represent average unfolding forces and error bars represent the mean ± SE.

On the other hand, unraveling of TM helix F through two different pathways common to both 3Glu and WT BR showed no change in the unfolding forces (Fig. S1, *D* and *E* in Data S1). The last structural segment of 3Glu BR, TM helix A, once again showed an increase in unfolding force (Fig. 4 *H*). This helix hosted mutation E9Q at its extracellular membrane-water interface.

Unfolding of three structural segments without any mutations, TM helices E and D together, TM helix E, and TM helix D via two pathways, occurred at similar forces in 3Glu and WT BR (Fig. S1, *F–I* in Data S1). However, unfolding of other structural segments without the mutations showed a change in their mechanical stabilities. For example, pairwise unfolding of TM helices B and C in 3Glu BR required considerably higher forces compared to WT BR (Fig. 4 *E*). In apparent agreement, the structural segments made of TM helix C and loop CB (Fig. 4 *F*), loop CB alone (Fig. 4 *G*), and the structural segment constituted by loop CB and TM helix B (Fig. S1 *L* in Data S1) all unfolded at slightly higher mechanical forces in 3Glu BR. The individual unfolding of helix C via one pathway occurred at marginally higher forces in 3Glu BR (Fig. S1 *J* in Data S1), whereas in the other pathway the unfolding forces were comparable to WT BR (Fig. S1 *K* in Data S1). Unfolding of single helix B via two different pathways required higher unfolding forces in 3Glu BR as compared to WT BR (Fig. S1, *M* and *N* in Data S1).

Specific structural segments of 3Glu BR change transition state positions

The positions of the transition states from the folded states, x_u, and the unfolding rates of the structural segments, k_u, define the energy barriers in an energy landscape (Fig. 5 *A*) (9,27). To determine if the mutations affect the unfolding energetics of BR we compared x_u and k_u of the transition state barriers established by the structural segments of 3Glu and WT BR (Table 2). Values of x_u and k_u of individual structural segments of WT BR were previously determined from DFS measurements (27).

The unfolding of TM helix G alone in 3Glu BR did not show a change in x_u on comparing with WT BR (Table 2). However, a difference in x_u was observed for loop GF. In the pathway where loop GF unfolded independently in the first step, preceding TM helix F, we noticed an increase in x_u from 0.15 ± 0.02 nm (WT BR) to 0.30 ± 0.05 nm (3Glu BR) (Table 2, loop GF—pathway 1, values in *bold*). This is interesting because mutations E204Q and E194Q were located within this loop. Although unfolding of loop GF with helix F in 3Glu BR via pathway 1 exhibited a similar $x_u = 0.37 \pm 0.07$ nm to that of WT BR (0.42 ± 0.32 nm), x_u determined for the same structural segment in pathway 2 was much lower for 3Glu BR (0.20 ± 0.04 nm) as compared to WT BR (0.37 ± 0.15 nm). These findings suggest that the transition state barrier of this structural segment depended on the unfolding pathway taken, and that the Gln mutations in 3Glu BR changed the transition state position of loop GF. The value of x_u for unfolding TM helix A with the N-terminus was 0.39 ± 0.04 nm for 3Glu BR as compared to 0.68 ± 0.1 nm for WT BR, thus decreasing the distance of the free energy minimum of the folded helix to the transition state barrier.

In addition to the structural segments containing the Gln mutations, significant changes in the unfolding transition state positions were also noticed for the unfolding of TM helices B and C together, TM helix C alone, TM helix B alone, and loop BC alone (see Table 2, values in *bold*).

Specific structural segments of 3Glu BR show different unfolding rates

We noticed somewhat unpredictable changes in the kinetic stability of individual structural segments upon introducing the mutations. Considering a change in the unfolding rate only when the difference between 3Glu and WT BR was at least

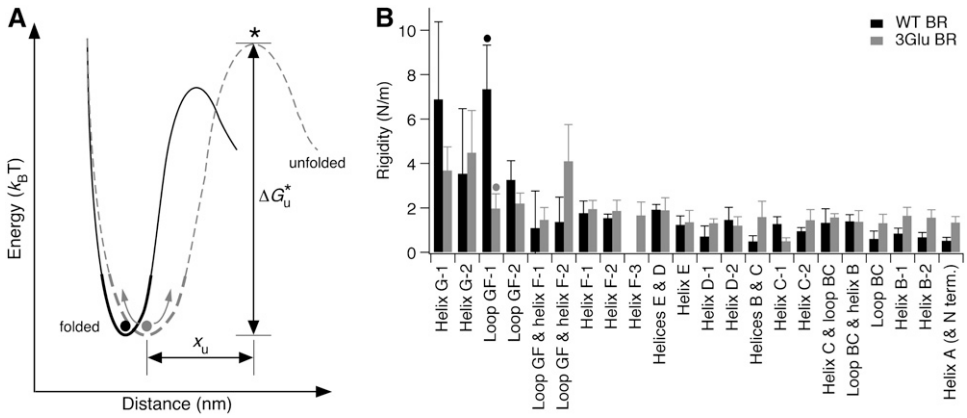

FIGURE 5 Stiffness of 3Glu and WT BR. (*A*) Model of an energy barrier separating the folded from the unfolded state of BR such as detected by DFS (27). The curvature of the potential well determines the conformational flexibility of a protein. A protein in a wide well has more freedom for conformational sampling. The solid and gray dots denote folded structures residing in potential wells, the gray arrows indicating the sampling of conformations. ΔG_u^* denotes the height of the energy barrier of the transition state (*) separating the folded from the unfolded state by a distance x_u. The rigidity of the structural segments hosting the Gln mutations was found to be lower than those of WT BR (*B*). Solid and gray dots in panel *B* show the dependence of the rigidity to the width of the potential well as depicted in *A*.

TABLE 2 Positions of transition states (x_u) and the unfolding rates (k_u) of structural segments of 3Glu and WT BR

	x_u (nm)		k_u (s^{-1})		κ (N/m)	
Structural segments	WT BR	3Glu BR	WT BR	3Glu BR	WT BR	3Glu BR
Helix G—Pathway 1	0.16 ± 0.04	0.21 ± 0.03	$4.7 \pm 8.9 \times 10^{-1}$	2.5 ± 2.1	6.9	3.7
Helix G—Pathway 2	0.22 ± 0.09	0.19 ± 0.04	$9.0 \pm 26.6 \times 10^{-1}$	2.7 ± 3.3	3.5	4.5
Loop GF—Pathway 1	**0.15 ± 0.02**	**0.30 ± 0.05**	1.8 ± 1.7	$4.3 \pm 5.4 \times 10^{-1}$	7.3	2.0
Loop GF—Pathway 2	0.23 ± 0.03	0.28 ± 0.03	$7.7 \pm 7.3 \times 10^{-1}$	$7.9 \pm 5.8 \times 10^{-1}$	3.3	2.2
Loop GF and helix F—Pathway 1	0.42 ± 0.32	0.37 ± 0.07	$7.9 \pm 53.6 \times 10^{-2}$	$2.9 \pm 6.0 \times 10^{-2}$	1.1	1.5
Loop GF and helix F—Pathway 2	**0.37 ± 0.15**	**0.20 ± 0.04**	$1.4 \pm 4.8 \times 10^{-1}$	2.1 ± 2.4	1.4	4.1
Helix F—Pathway 1	0.32 ± 0.05	0.30 ± 0.03	$3.1 \pm 3.2 \times 10^{-1}$	$5.9 \pm 4.7 \times 10^{-1}$	1.8	1.9
Helix F—Pathway 2	0.34 ± 0.02	0.31 ± 0.04	$4.2 \pm 1.9 \times 10^{-1}$	$3.4 \pm 3.4 \times 10^{-1}$	1.5	1.9
Helix F—Pathway 3		0.33 ± 0.06		$3.0 \pm 4.5 \times 10^{-1}$		1.7
Helices E and D	0.33 ± 0.02	0.34 ± 0.05	$9.8 \pm 7.4 \times 10^{-3}$	$2.8 \pm 4.6 \times 10^{-3}$	1.9	1.9
Helix E	0.44 ± 0.07	0.42 ± 0.08	$2.3 \pm 5.3 \times 10^{-4}$	$2.5 \pm 7.2 \times 10^{-4}$	1.2	1.3
Helix D—Pathway 1	0.58 ± 0.19	0.39 ± 0.03	$\mathbf{2.1 \pm 9.4 \times 10^{-4}}$	$\mathbf{3.0 \pm 2.2 \times 10^{-2}}$	0.7	1.3
Helix D—Pathway 2	0.36 ± 0.07	0.42 ± 0.07	$\mathbf{1.1 \pm 1.8 \times 10^{-1}}$	$\mathbf{7.4 \pm 14.3 \times 10^{-3}}$	1.5	1.2
Helices B and C	**0.69 ± 0.18**	**0.36 ± 0.08**	$\mathbf{4.2 \pm 13.6 \times 10^{-4}}$	$\mathbf{1.3 \pm 3.0 \times 10^{-2}}$	0.5	1.6
Helix C—Pathway 1	**0.39 ± 0.05**	**0.75 ± 0.11**	$\mathbf{5.9 \pm 5.1 \times 10^{-2}}$	$\mathbf{1.2 \pm 3.5 \times 10^{-6}}$	1.3	0.5
Helix C—Pathway 2	0.47 ± 0.04	0.37 ± 0.06	$8.9 \pm 6.8 \times 10^{-3}$	$3.5 \pm 4.7 \times 10^{-2}$	0.9	1.4
Helix C and loop BC	0.38 ± 0.09	0.36 ± 0.02	$7.3 \pm 13.4 \times 10^{-2}$	$1.9 \pm 0.9 \times 10^{-2}$	1.3	1.6
Loop BC and helix B	0.37 ± 0.04	0.39 ± 0.07	$9.1 \pm 7.7 \times 10^{-2}$	$8.8 \pm 16.7 \times 10^{-3}$	1.4	1.4
Loop BC	**0.61 ± 0.18**	**0.39 ± 0.06**	$1.4 \pm 4.5 \times 10^{-3}$	$3.1 \pm 4.3 \times 10^{-2}$	0.6	1.3
Helix B—Pathway 1	**0.48 ± 0.07**	**0.34 ± 0.04**	$6.6 \pm 6.8 \times 10^{-2}$	$9.8 \pm 8.3 \times 10^{-2}$	0.8	1.6
Helix B—Pathway 2	**0.55 ± 0.09**	**0.35 ± 0.04**	$1.9 \pm 2.7 \times 10^{-2}$	$8.7 \pm 8.2 \times 10^{-2}$	0.7	1.6
Helix A (and N-terminus)	**0.68 ± 0.1**	**0.39 ± 0.04**	$\mathbf{1.9 \pm 3.6 \times 10^{-4}}$	$\mathbf{1.9 \pm 2.0 \times 10^{-2}}$	0.5	1.3

Values of x_u and k_u of 3Glu BR are compared to those of WT BR. The criteria chosen for determining a significant difference in the x_u and k_u values was as follows: For the x_u values, we determined whether these were within the standard errors of each other. If so, those were taken to be similar. A difference in the k_u for a structural segment was considered only if the values were at least two orders-of-magnitude different between 3Glu and WT BR. The x_u and k_u values that showed a significant difference are highlighted in bold. The numbers after the structural segments denote the pathways in which they unfolded.

two orders of magnitude (32), no significant change in the k_u values was observed. This was the case for all the structural segments with mutations except for TM helix A, which unfolded at a rate of $1.9 \times 10^{-2}\ s^{-1}$ in 3Glu BR compared to $1.9 \times 10^{-4}\ s^{-1}$ in WT BR. The Gln mutations thus decreased the kinetic stability of helix A from ~10,000 s to ~100 s (Table 2, values in *bold*).

Gln mutations change the rigidity of structural segments

The thermally averaged distance between the folded state and the transition state, x_u, also provides information on the physical characteristics of a protein. Brittle structural segments withstand force for smaller extensions before reaching their transition states and thus have a smaller value of x_u. Segments that are more compliant are resistant to the applied force for larger extensions before reaching the transition state and have a larger value of x_u. For example, a larger x_u of 0.30 nm observed for loop GF in 3Glu BR over 0.15 nm in WT BR implies that under similar force this loop could be stretched at least two times more in the mutant before it would start to unfold. Introducing a mutation which alters the interactions in a protein and hence the position of the transition state, therefore, affects the physical properties of a structural segment.

Considering a parabolic potential for a partially folded intermediate state and a sharp transition barrier (as suggested by DFS data) for the structural segments of 3Glu and WT BR, we calculated the spring constant, κ, of each structural segment using the formula, $\kappa = 2 \times \Delta G_u^*/x_u^2$ (Fig. 5 *A*) (see Materials and Methods) (11,38). The value of κ was taken as a measure of rigidity. Crucially, we define rigidity of a structural segment as its ability to resist deformation, i.e., unfolding, until its yield point, i.e., the transition state, where it starts to unfold under an applied force. In this regard, it is important to mention that the measure of rigidity of a structural segment is not of its unfolded polypeptide chain but that of an average population of molecules between the folded ground state and its transition state.

A clear assumption of the phenomenological and the microscopic models in the calculation of the energy landscape parameters, x_u and ΔG_u^*, is that the system diffuses in a harmonic potential well with a single sharp energy barrier (9,29,31). We have carried over these assumptions for the calculation of the rigidity of the structural segments. In addition, the phenomenological model of Evans' assumes a stationary sharp transition barrier under increasing loading rates (8,9). A linear dependence of $\langle F \rangle$ on the $\log_e$(loading rate) from our data supports the assumption of a single transition barrier. Because the distance between the folded states and the transition states is less than two amino acids (the measured values of x_u in Table 2), we consider the deformation of the structural segments to be small, and hence the behavior of structural segments to be linear under force in this range. This assumption may not be true for the entire force range.

Because a protein is anisotropic in nature, the local thermal fluctuations play an important role in determining its energy landscape. Interestingly, we found the rigidity of a structural segment to depend on its unfolding pathway (Fig. 5 *B*, Table 2). A decrease in rigidity was observed for TM helix G in pathway 1, whereas no significant change was observed in pathway 2. Similarly, the rigidity of loop GF, and the structural segment constituted of loop GF and TM helix F together, was found to vary in their two different unfolding pathways. A pathway-dependent rigidity change is an indication of the heterogeneity in the protein population due to dynamic changes in the protein structure. Without excluding completely the effect of E9Q mutation, it could be suggested that mutations E194Q and E204Q at the two ends of loop GF altered the stiffness of this structural region of the membrane protein. In concurrence with this, it was shown by ^{13}C NMR measurements that simultaneous E194Q/E204Q mutations lead to a substantial increase in the mobility of the extracellular region of BR (44). Mutation E9Q increased the rigidity of TM helix A.

Besides the mutations containing structural segments, a change in the rigidity of other structural segments was also observed. Structural segments constituted by helices B and C, helix B, and loop BC exhibited increased rigidity in 3Glu BR as compared to WT BR (Fig. 5 *B*, Table 2). Thus, the mutations affected the mechanical properties of not only the structural segments in which they were located but also of other structural segments.

DISCUSSION

Mutating key amino-acid residues changes inter- and intramolecular interactions of proteins. Understanding the mechanisms by which mutations alter interactions that modify the structure and function of membrane proteins builds the key to understanding the molecular origin of many human diseases (49) and for many nanobiotechnological applications (50–52). The concept of energy landscape has revolutionized our understanding of how localized transitions in interactions guide energetically favorable pathways toward functional biological processes (53–55). Its most important point that biomolecular processes can be guided via multiple pathways rather than through a single one has been frequently demonstrated (53,56–59). The coexistence of multiple unfolding pathways observed for BR (23) and for other membrane proteins (7) by SMFS are excellent examples, which support the concept of funneled energy landscapes.

The forced unfolding of WT BR by SMFS revealed 15 coexisting unfolding pathways (Table 1) (23), each one being populated differently. Besides the unfolding pathways of TM helices G and F observed previously in WT BR (23), we observed one new unfolding pathway for these helices in 3Glu BR. It is of significant interest to note that the occurrence of this new unfolding pathway involved secondary structure elements embedding the mutations. Since no other structural region of 3Glu BR showed the presence of a new pathway, we attribute the appearance of this pathway to localized changes in interactions occurring due, mainly, to the substitution of Glu at positions 194 and 204 with Gln. It was shown that mutating Glu at least at two sites, 194 and 204, induces major conformational changes (44). It could be suggested that the new unfolding pathway is a result of the altered conformation in the BR structure due to mutations E194Q and E204Q. However, the contribution of E9Q in the alteration of interactions cannot be completely discarded owing to its location in the extracellular region. Recently, we have reported the effect of mutating single amino acids, not known to be involved in the functioning of BR, on the energy landscape of BR (40). In the previous study, although a change in the populations of the unfolding intermediates was observed for both structural segments hosting the point mutations and those without the point mutations, no new unfolding intermediate was detected in any of the five single point mutants as compared to WT BR. On the other hand a new unfolding intermediate, hitherto not observed in WT BR nor the previously studied single point mutants, was detected in 3Glu BR. None of the five mutant proteins studied previously was known to have a considerable change in bonding pattern (60,61), as opposed to 3Glu BR studied here, which has an altered hydrogen-bond network on the extracellular side. It may, therefore, be speculated that amino acids involved in the important functional conformations of a protein may also play a role in defining its folding dynamics.

A change in transition state positions, unfolding rates, and occurrence probability was also observed for the structural segments without any mutations in 3Glu BR. These changes can be attributed to long-range interactions between amino acids far apart in sequence but closer in space in the membrane protein. But how do changes in interactions change the unfolding pathways of the protein along the energy landscape? The changing shape of the individual energy barriers allows us to approach mechanistic insights into this behavior. The energy barriers of the unfolding intermediates are molded by the interactions of the membrane protein. The interactions introduced by Gln mutations change the characteristic properties of the energy barriers stabilizing the structural segments in BR (Table 2). The rather subtle changes in the positions of the transition states and the kinetic stability of the structural segments (Table 1), introduced by the mutations, force the protein to populate certain unfolding pathways over others (Fig. 6).

The distance between the folded and the transition state of a structural segment defines the mechanical properties of the structural segment. A larger distance between the folded state and the transition state suggests that the structural segment incorporates more conformational substates, while a shorter distance implies a reduced number of conformation defining substates of the segment. Consequently, a structure with more conformational substates indicates its flexible nature, whereas a mechanically rigid structure exhibits fewer substates (62).

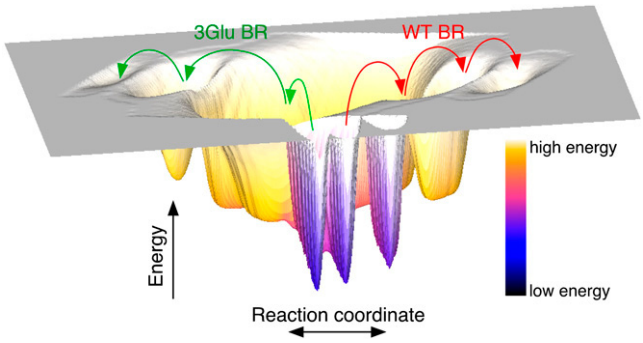

FIGURE 6 A schematic diagram showing unfolding pathways contoured on the energy landscape. The basins in the energy landscape, where the 3Glu and WT BR reside, dictate the structural interactions and hence the mechanical characteristics of these proteins. Mutations E9Q/E194Q/E204Q in BR (3Glu BR) introduce interactions that alter the wells and barriers in the energy landscape. This changes the mechanical and kinetic stability of specific structural regions within the proton pump. Consequently, it is observed that the mutated BR populates unfolding pathways differently. Since unfolding as well as the function of the proton pump can be described by the energy landscape, this leads to the conclusion that the altered energy barriers forces different functional states of the protein to chart out different regions in the energy landscape. The red and green arrows represent the unfolding pathways of WT BR and 3Glu BR, respectively, contouring the energy landscape. The troughs in the diagram represent the potential wells in the energy landscape.

Thus, the width of the potential well defines the rigidity of a structural segment. The Gln mutations investigated in this work shifted the transition states of several structural segments toward or away from the folded intermediate state. The most apparent decrease in rigidity involved mutations hosting secondary structure elements helix G and loop GF. These secondary structure elements also showed reduced mechanical stability. On the other hand, the rest of the structural segments, including helix A with mutation E9Q, exhibited an increase in mechanical rigidity and stability. A highly structured hydrogen-bonded network involving several water molecules and amino-acid residues in the extracellular region of WT BR has been proposed (63–65). Substituting Glu by Gln not only abolishes ionization but also decreases the hydrogen-bonding ability due to the lower water-binding capacity of Gln against Glu. This considerably weakens the water network distribution by decreasing the number of water molecules in the network (19). The three mutated extracellular Glu side chains, E9, E194, and E204, are also involved in cation binding (12) as demonstrated by a fourfold increase in the Ca^{2+} concentration needed to restore the purple form of 3Glu BR compared to WT BR. It is intuitive that the water molecules forming hydrogen bonds, and the cations, would influence the interactions and, thus, the structural rigidity of these regions differently.

The conformational substates of a protein are trapped in one of the many coexisting potential wells (Fig. 5 *A*). The curvature of the potential well, in which the protein resides, is dictated by the interactions the protein has to overcome to cross the transition state. Disturbing the hydrogen-bond network and consequently the mechanical properties of different structural regions may in turn affect the ability of BR to switch conformations required for pumping protons across the membrane (66). The dynamic changes as detected by the different unfolding pathways and rigidity in the 3Glu BR mutant as compared to WT BR are in line with the structural and functional properties of the mutated extracellular residues (12,44). Structurally, accessibility to hydroxylamine appears to be ~100 times increased in 3Glu BR as compared to WT BR (C. Sanz, T. Lazarova, E. Querol, and E. Padrós, unpublished experiments), indicating an increased flexibility of the extracellular region. The quadruple mutant E9Q/E74Q/E194Q/E204Q shows a similar behavior to the triple mutant, whereas the double mutant E194Q/E204Q is more stable (44). Functionally, the M intermediate yield of 3Glu BR is decreased to <20% of WT BR (C. Sanz, T. Lazarova, E. Querol, and E. Padrós, unpublished experiments), showing a perturbed proton transport mechanism that may be, in part, due to to the more loose conformation of the extracellular region.

OUTLOOK

The advantage of SMFS against other conventional methods studying the thermal or chemical stability of BR is that SMFS reveals detailed insights into the strength of interactions stabilizing single structural segments of BR, reveals details of the underlying energy landscape, tracks the population of unfolding pathways, and most importantly can be employed for experiments on BR in the native purple membrane in a relevant buffer solution. The substitution of Glu by Gln, investigated in this work, altered interactions of specific structural segments of BR. These interactions changed the transition states and rates of energy barriers in the energy landscape of the proton pump. We could trace that changing the mechanical properties and kinetics of structural regions in BR forces the protein to populate different unfolding pathways in the energy landscape. In other words, the Gln substitutions funneled the proton pump differently through the energy landscape.

The approach described here allows us to trace how mutants stabilize certain regions and thereby exclude certain unfolding pathways against others. Screening of mutants that shift low energy barriers toward higher energies may represent one possibility to select and to improve the bionanotechnological applicability of BR. Because both unfolding and proton pumping of BR include a series of structural changes, such as described by the pathways chosen in the energy landscape, we speculate that our findings may also have direct implications in the proton pumping mechanism of BR.

SUPPLEMENTARY MATERIAL

To view all of the supplemental files associated with this article, visit www.biophysj.org.

The authors thank Carolina Sanz and Neus Ontiveros for help in the preparation of 3Glu BR, and Dirk Labudde for help with analysis of unfolding pathways (Fig. S2 in Data S1).

This work was supported by the Deutsche Forschungsgemeinschaft, the European Union and the free state of Saxony. V.R. acknowledges support from National Science Foundation, Wallace H. Coulter Foundation, Harvard Medical School. Research in E.P.'s laboratory has been supported by the Dirección General de Investigación grant No. BFU2006-04656/BMC.

REFERENCES

1. Oesterhelt, D., and W. Stoeckenius. 1973. Functions of a new photoreceptor membrane. *Proc. Natl. Acad. Sci. USA*. 70:2853–2857.
2. Henderson, R., and P. N. T. Unwin. 1975. Three-dimensional model of purple membrane obtained by electron microscopy. *Nature*. 257: 28–32.
3. Büldt, G., K. Konno, K. Nakanishi, H. J. Ploehn, B. N. Rao, and N. A. Dencher. 1991. Heavy-atom labeled retinal analogues located in bacteriorhodopsin by x-ray diffraction. *Photochem. Photobiol*. 54: 873–879.
4. Jubb, J. S., D. L. Worcester, H. L. Crespi, and G. Zaccai. 1984. Retinal location in purple membrane of *Halobacterium halobium*: a neutron diffraction study of membranes labeled *in vivo* with deuterated retinal. *EMBO J*. 3:1455–1461.
5. Oesterhelt, D. 1973. Reversible dissociation of the purple complex in bacteriorhodopsin and identification of 13-*cis* and all-*trans*-retinal as its chromophores. *Eur. J. Biochem*. 40:453–463.
6. Lanyi, J. K. 2004. Bacteriorhodopsin. *Annu. Rev. Physiol*. 66:665–688.
7. Kedrov, A., H. Janovjak, K. T. Sapra, and D. J. Muller. 2007. Deciphering molecular interactions of native membrane proteins by single-molecule force spectroscopy. *Annu. Rev. Biophys. Biomol. Struct*. 36:233–260.
8. Evans, E. 1998. Energy landscapes of biomolecular adhesion and receptor anchoring at interfaces explored with dynamic force spectroscopy. *Faraday Discuss*. 111:1–16.
9. Evans, E. 2001. Probing the relation between force-lifetime-and chemistry in single molecular bonds. *Annu. Rev. Biophys. Biomol. Struct*. 30:105–128.
10. Sapra, K. T., P. S. Park, K. Palczewski, and D. J. Muller. 2008. Mechanical properties of bovine rhodopsin and bacteriorhodopsin: possible roles in folding and function. *Langmuir*. 24:1330–1337.
11. Dietz, H., F. Berkemeier, M. Bertz, and M. Rief. 2006. Anisotropic deformation response of single protein molecules. *Proc. Natl. Acad. Sci. USA*. 103:12724–12728.
12. Sanz, C., M. Marquez, A. Peralvarez, S. Elouatik, F. Sepulcre, E. Querol, T. Lazarova, and E. Padros. 2001. Contribution of extracellular Glu residues to the structure and function of bacteriorhodopsin. Presence of specific cation-binding sites. *J. Biol. Chem*. 276:40788–40794.
13. Luecke, H., H.-T. Richter, and J. K. Lanyi. 1998. Proton transfer pathways in bacteriorhodopsin at 2.3 Angstrom resolution. *Science*. 280:1934–1937.
14. Lanyi, J. K. 1997. Mechanisms of ion transport across membranes. *J. Biol. Chem*. 272:31209–31212.
15. Brown, L. S., J. Sasaki, H. Kandori, A. Maeda, R. Needleman, and J. K. Lanyi. 1995. Glutamic acid 204 is the terminal proton release group at the extracellular surface of bacteriorhodopsin. *J. Biol. Chem*. 270:27122–27126.
16. Bondar, A. N., M. Elstner, S. Suhai, J. C. Smith, and S. Fischer. 2004. Mechanism of primary proton transfer in bacteriorhodopsin. *Structure*. 12:1281–1288.
17. Sampogna, R. V., and B. Honig. 1996. Electrostatic coupling between retinal isomerization and the ionization state of Glu-204: a general mechanism for proton release in bacteriorhodopsin. *Biophys. J*. 71: 1165–1171.
18. Richter, H. T., L. S. Brown, R. Needleman, and J. K. Lanyi. 1996. A linkage of the pK_as of Asp-85 and Glu-204 forms part of the reprotonation switch of bacteriorhodopsin. *Biochemistry*. 35:4054–4062.
19. Sanz, C., T. Lazarova, F. Sepulcre, R. Gonzalez-Moreno, J. L. Bourdelande, E. Querol, and E. Padros. 1999. Opening the Schiff base moiety of bacteriorhodopsin by mutation of the four extracellular Glu side chains. *FEBS Lett*. 456:191–195.
20. Lazarova, T., C. Sanz, E. Querol, and E. Padros. 2000. Fourier transform infrared evidence for early deprotonation of Asp^{85} at alkaline pH in the photocycle of bacteriorhodopsin mutants containing E194Q. *Biophys. J*. 78:2022–2030.
21. Oesterhelt, D., and W. Stoeckenius. 1974. Isolation of the cell membrane of *Halobacterium halobium* and its fraction into red and purple membrane. *Methods Enzymol*. 31:667–678.
22. Oesterhelt, F., D. Oesterhelt, M. Pfeiffer, A. Engel, H. E. Gaub, and D. J. Müller. 2000. Unfolding pathways of individual bacteriorhodopsins. *Science*. 288:143–146.
23. Müller, D. J., M. Kessler, F. Oesterhelt, C. Möller, D. Oesterhelt, and H. E. Gaub. 2002. Stability of bacteriorhodopsin α-helices and loops analyzed by single-molecule force spectroscopy. *Biophys. J*. 83:3578–3588.
24. Kessler, M., and H. E. Gaub. 2006. Unfolding barriers in bacteriorhodopsin probed from the cytoplasmic and the extracellular side by AFM. *Structure*. 14:521–527.
25. Florin, E.-L., M. Rief, H. Lehmann, M. Ludwig, C. Dornmair, V. T. Moy, and H. E. Gaub. 1995. Sensing specific molecular interactions with the atomic force microscope. *Biosens. Bioelectron*. 10: 895–901.
26. Butt, H.-J., and M. Jaschke. 1995. Calculation of thermal noise in atomic force microscopy. *Nanotechnology*. 6:1–7.
27. Janovjak, H., J. Struckmeier, M. Hubain, A. Kedrov, M. Kessler, and D. J. Müller. 2004. Probing the energy landscape of the membrane protein bacteriorhodopsin. *Structure*. 12:871–879.
28. Rief, M., M. Gautel, F. Oesterhelt, J. M. Fernandez, and H. E. Gaub. 1997. Reversible unfolding of individual titin immunoglobulin domains by AFM. *Science*. 276:1109–1112.
29. Dudko, O. K., G. Hummer, and A. Szabo. 2006. Intrinsic rates and activation free energies from single-molecule pulling experiments. *Phys. Rev. Lett*. 96:108101–108104.
30. Dudko, O. K., A. E. Filippov, J. Klafter, and M. Urbakh. 2003. Beyond the conventional description of dynamic force spectroscopy of adhesion bonds. *Proc. Natl. Acad. Sci. USA*. 100:11378–11381.
31. Hummer, G., and A. Szabo. 2003. Kinetics from nonequilibrium single-molecule pulling experiments. *Biophys. J*. 85:5–15.
32. Best, R. B., S. B. Fowler, J. L. Toca-Herrera, and J. Clarke. 2002. A simple method for probing the mechanical unfolding pathway of proteins in detail. *Proc. Natl. Acad. Sci. USA*. 99:12143–12148.
33. Bell, G. I. 1978. Models for the specific adhesion of cells to cells. *Science*. 200:618–627.
34. Evans, E. 1999. Looking inside molecular bonds at biological interfaces with dynamic force spectroscopy. *Biophys. Chem*. 82: 83–97.
35. Evans, E., and K. Ritchie. 1997. Dynamic strength of molecular adhesion bonds. *Biophys. J*. 72:1541–1555.
36. Dietz, H., and M. Rief. 2004. Exploring the energy landscape of GFP by single-molecule mechanical experiments. *Proc. Natl. Acad. Sci. USA*. 101:16192–16197.
37. Bieri, O., J. Wirz, B. Hellrung, M. Schutkowski, M. Drewello, and T. Kiefhaber. 1999. The speed limit for protein folding measured by triplet-triplet energy transfer. *Proc. Natl. Acad. Sci. USA*. 96:9597–9601.
38. Schlierf, M., and M. Rief. 2005. Temperature softening of a protein in single-molecule experiments. *J. Mol. Biol*. 354:497–503.
39. Howard, J. 2001. Mechanics of Motor Proteins and the Cytoskeleton. Sinauer, Sunderland, MA.
40. Sapra, K. T., G. P. Balasubramanian, D. Labudde, J. U. Bowie, and D. J. Muller. 2008. Point mutations in membrane proteins reshape energy landscape and populate different unfolding pathways. *J. Mol. Biol*. 376:1076–1090.

41. Contera, S. A., V. Lemaitre, M. R. de Planque, A. Watts, and J. F. Ryan. 2005. Unfolding and extraction of a transmembrane α-helical peptide: dynamic force spectroscopy and molecular dynamics simulations. *Biophys. J.* 89:3129–3140.

42. Janovjak, H., A. Kedrov, D. A. Cisneros, K. T. Sapra, and D. J. Müller. 2006. Imaging and detecting molecular interactions of single transmembrane proteins. *Neurobiol. Aging*. 27:546–561.

43. Sapra, K. T., H. Besir, D. Oesterhelt, and D. J. Muller. 2006. Characterizing molecular interactions in different bacteriorhodopsin assemblies by single-molecule force spectroscopy. *J. Mol. Biol.* 355:640–650.

44. Saito, H., S. Yamaguchi, K. Ogawa, S. Tuzi, M. Marquez, C. Sanz, and E. Padros. 2004. Glutamic acid residues of bacteriorhodopsin at the extracellular surface as determinants for conformation and dynamics as revealed by site-directed solid-state ^{13}C NMR. *Biophys. J.* 86:1673–1681.

45. Janovjak, H., M. Kessler, D. Oesterhelt, H. E. Gaub, and D. J. Müller. 2003. Unfolding pathways of native bacteriorhodopsin depend on temperature. *EMBO J.* 22:5220–5229.

46. Kedrov, A., M. Krieg, C. Ziegler, W. Kuhlbrandt, and D. J. Müller. 2005. Locating ligand binding and activation of a single antiporter. *EMBO Rep.* 6:668–674.

47. Park, P. S., K. T. Sapra, M. Kolinski, S. Filipek, K. Palczewski, and D. J. Muller. 2007. Stabilizing effect of Zn^{2+} in native bovine rhodopsin. *J. Biol. Chem.* 282:11377–11385.

48. Janovjak, H., H. Knaus, and D. J. Muller. 2007. Transmembrane helices have rough energy surfaces. *J. Am. Chem. Soc.* 129:246–247.

49. Nagy, J. K., and C. R. Sanders. 2004. Destabilizing mutations promote membrane protein misfolding. *Biochemistry.* 43:19–25.

50. Astier, Y., H. Bayley, and S. Howorka. 2005. Protein components for nanodevices. *Curr. Opin. Chem. Biol.* 9:576–584.

51. Bayley, H., and L. Jayasinghe. 2004. Functional engineered channels and pores. *Mol. Membr. Biol.* 21:209–220.

52. Leifert, W. R., A. L. Aloia, O. Bucco, R. V. Glatz, and E. J. McMurchie. 2005. G-protein-coupled receptors in drug discovery: nanosizing using cell-free technologies and molecular biology approaches. *J. Biomol. Screen.* 10:765–779.

53. Onuchic, J. N., P. G. Wolynes, Z. Luthey-Schulten, and N. D. Socci. 1995. Toward an outline of the topography of a realistic protein-folding funnel. *Proc. Natl. Acad. Sci. USA.* 92:3626–3630.

54. Wolynes, P. G., J. N. Onuchic, and D. Thirumalai. 1995. Navigating the folding routes. *Science.* 267:1619–1620.

55. Dill, K. A., and H. S. Chan. 1997. From Levinthal to pathways to funnels. *Nat. Struct. Biol.* 4:10–19.

56. Bryngelson, J. D., J. N. Onuchic, N. D. Socci, and P. G. Wolynes. 1995. Funnels, pathways, and the energy landscape of protein folding: a synthesis. *Proteins.* 21:167–195.

57. Jahn, T. R., and S. E. Radford. 2005. The Yin and Yang of protein folding. *FEBS J.* 272:5962–5970.

58. Boehr, D. D., D. McElheny, H. J. Dyson, and P. E. Wright. 2006. The dynamic energy landscape of dihydrofolate reductase catalysis. *Science.* 313:1638–1642.

59. Frederick, K. K., M. S. Marlow, K. G. Valentine, and A. J. Wand. 2007. Conformational entropy in molecular recognition by proteins. *Nature.* 448:325–329.

60. Faham, S., D. Yang, E. Bare, S. Yohannan, J. P. Whitelegge, and J. U. Bowie. 2004. Side-chain contributions to membrane protein structure and stability. *J. Mol. Biol.* 335:297–305.

61. Yohannan, S., S. Faham, D. Yang, J. P. Whitelegge, and J. U. Bowie. 2004. The evolution of transmembrane helix kinks and the structural diversity of G protein-coupled receptors. *Proc. Natl. Acad. Sci. USA.* 101:959–963.

62. Oliveberg, M., and P. G. Wolynes. 2006. The experimental survey of protein-folding energy landscapes. *Q. Rev. Biophys.* 38:245–288.

63. Belrhali, H., P. Nollert, A. Royant, C. Menzel, J. P. Rosenbusch, E. M. Landau, and E. Pebay-Peyroula. 1999. Protein, lipid and water organization in bacteriorhodopsin crystals: a molecular view of the purple membrane at 1.9 A resolution. *Struct. Fold. Des.* 7:909–917.

64. Luecke, H., B. Schobert, H. T. Richter, J. P. Cartailler, and J. K. Lanyi. 1999. Structure of bacteriorhodopsin at 1.55 A resolution. *J. Mol. Biol.* 291:899–911.

65. Dencher, N. A., H. J. Saas, and G. Buldt. 2000. Water and bacteriorhodopsin: structure, dynamics and function. *Biochim. Biophys. Acta.* 1460:192–203.

66. Reat, V., H. Patzelt, M. Ferrand, C. Pfister, D. Oesterhelt, and G. Zaccai. 1998. Dynamics of different functional parts of bacteriorhodopsin: H-^{2}H labeling and neutron scattering. *Proc. Natl. Acad. Sci. USA.* 95:4970–4975.

67. Thavasi, V., T. Lazarova, S. Filipek, M. Kolinski, E. Querol, A. Kumar, S. Ramakrishna, E. Padrós, V. Renugopalakrishnan. Study on the feasibility of bacteriorhodopsin as bio-photosensitizer in excitonic solar cell: a first report. *J. Nanosci.* and *Nanotechnol.* 2008. In press.